Chapter 13

OTHER COMPONENTS AND VARIATIONS

The preceding chapters have considered the basic aerodynamic design and analysis functions relative to typical axial-flow compressor configurations. Blade row, stage and compressor design and analysis have been considered in the context of the compressor flow path from the first blade row to the last, including operation at off-design speeds and mass flow rates. This chapter addresses other design and analysis functions that are often required by the specific application. One obvious consideration for industrial axial-flow compressors is dictated by the need to supply the compressor discharge flow to the process through a discharge pipe, typically exiting in the radial direction. This requires the design and analysis of an exhaust diffuser and flow collection system, which can have significant influence on the overall performance of the compressor. Another important consideration is the use of adjustable inlet guide vanes and stators as a means of improving the surge margin. Normally this provides a substantially better surge margin at mass flows that are significantly less than the design flow than can be achieved with simple variable speed operation. Indeed, variable geometry is an essential requirement for many industrial compressor applications. The influence of surface roughness on performance is discussed to provide a basis for its evaluation when required. Finally, the axial-centrifugal compressor is briefly discussed. This configuration includes a centrifugal compressor stage following a series of typical axial-flow compressor stages. Under appropriate operating conditions, this can offer significant cost and performance benefits.

NOMENCLATURE

A = passage area
A_m = maximum, stall-free passage area
B = fractional area blockage
B_{BL} = boundary layer fractional area blockage
B_{SEP} = minimum fractional area blockage due to flow separation
b = passage width
C = absolute velocity
c_p = static pressure recovery coefficient
c_f = skin friction coefficient
D = $2\tan\theta_C$

D_m = limiting value of D for low diffusion losses
d = characteristic diameter for Reynolds number definition
d_H = hydraulic diameter
E = diffusion efficiency parameter
e = peak-to-valley surface roughness
e_{rms} = root-mean-square surface roughness
F = normalized stagger angle adjustment
H = total enthalpy
h = static enthalpy
I_C = passage curvature loss term
I_D = passage diffusion loss term
i = adjustable blade row number
L = diffuser meridional length and scroll/collector flow path length
m = meridional coordinate
$\dot{m}$ = mass flow rate
N = total number of adjustable blade rows
n = exponent in power-law stagger adjustment distribution
P = pressure
R = ratio of stagger angle adjustments on successive stationary rows
Re = Reynolds number
r = radius
SP = scroll/collector sizing parameter
U = local blade speed = ωr
γ = stagger angle
δ = boundary layer thickness
ε = hub-to-shroud radius ratio
θ = polar angle
θ_C = diffuser divergence angle
κ_m = stream surface curvature
μ = gas viscosity
ρ = gas density
τ_w = wall shear stress
ϕ = flow coefficient = C_m/U; also, slope angle of mean stream surface with the axial direction
ϕ_0 = characteristic inlet flow coefficient
ω = rotation speed, radians/sec.
$\overline{\omega}$ = total pressure loss coefficient

Subscripts

0 = parameter at a stage inlet
1 = parameter at the diffuser inlet
2 = parameter at the diffuser exit
3 = parameter at the scroll/collector full-collection plane
4 = parameter at the exit cone discharge flange
l = laminar condition
ex = exit cone parameter

m = meridional component
r = fully rough wall condition
s = smooth wall value
sf = skin friction parameter
t = total thermodynamic condition or turbulent condition
tip = blade tip parameter
θ = tangential component

13.1 ADJUSTABLE BLADE ROWS

There are two important considerations when using adjustable stationary blade rows: The number of adjustable blade rows to be used must be selected and the distribution of the stagger angle adjustments among those rows must be established. These decisions can be conveniently made using a performance analysis such as that described in Chapter 9. It is relatively easy to include the capability to impose adjustments to the base stagger angles for specific blade rows. It is most convenient to specify those adjustments as a fraction of a reference stagger angle adjustment, e.g., the adjustment to be made to the first adjustable blade row. If that is done, performance predictions for a series of different adjustable blade row settings can be accomplished by simply changing the value of the reference stagger angle adjustment.

The most obvious design strategy would be to select one specific setting of the adjustable blades, such as the most extreme adjustment to be used, and optimize the distribution of the adjustments among all adjustable rows. In practice, that is a rather ineffective approach. Adjustable blade rows can produce rather extreme incidence angles on both rotors and stators to substantially increase the uncertainty of the performance analysis and the reliability of any estimate of the surge limit based on that analysis. If an adjustment strategy is established to optimize the most extreme adjustment, prediction of an overall map of adjustments is likely to be totally lacking in credibility. The most common result is to find the estimated surge margin deteriorating at adjustments even slightly different from the optimized adjustment. The real problem lies with the performance predictions for the optimized adjustment. Off-design performance analysis at extreme incidence angles involves too much uncertainty for the optimized adjustments to really be believable. The very precise stage matching chosen to enhance surge margin is very unlikely to be achieved in the actual compressor. Hence the designer who attempts such an optimization strategy is really exceeding the capabilities of off-design performance analysis technology. In effect, that is an excellent way to expose all of the weaknesses of the performance analysis, which is hardly a good basis for design. Even if the performance analysis could accurately model this situation, a surge line that achieves enhanced surge margin very local to one adjustment setting would not be very useful.

A better approach is to establish general stagger-angle adjustment distributions for this purpose and evaluate the results with the performance analysis. These general distributions can offer considerable flexibility and yet be very unlikely to produce a misleading "optimum stage matching" distribution. Three general distributions found to be effective for this purpose will be presented and

demonstrated here. If there are N adjustable blades, let F_i represent the adjustment to the ith adjustable blade row in the form

$$\Delta\gamma_i = \Delta\gamma_{ref} F_i \tag{13-1}$$

where $\Delta\gamma_{ref}$ is the reference adjustment, which will be assumed to be the adjustment to the first adjustable row, such that $F_1 = 1$. One useful distribution is a simple linear variation such that the adjustment to the stator following the last adjustable stator would be zero, i.e.,

$$F_i = (N + 1 - i)/N \tag{13-2}$$

A simple variation on the linear distribution will be referred to as the power-law distribution, given by

$$F_i = [(N + 1 - i)/N]^n \tag{13-3}$$

Another useful distribution is the fractional distribution, which simply adjusts each blade row as a specified ratio, R, of the adjustment on the preceding adjustable blade, i.e.,

$$F_i = R^{(i-1)} \tag{13-4}$$

Figure 13-1 illustrates these three stagger angle distributions for a case where $N = 7$. The linear and fractional distributions are adequate for most applications, but the power-law distribution provides some additional flexibility if needed. When these models are incorporated into the performance analysis, investigation of alternatives for adjustable geometry is rather simple. It is only necessary to specify the adjustment distribution type, the number of adjustable blade rows and the stagger angle adjustment on the first row. Simply varying the last parameter permits analysis of alternate settings of the adjustable rows.

The ten-stage axial-flow compressor design of Fig.10-38 will be employed to illustrate the use of adjustable stationary blades. This is a repeating stage design with inlet guide vanes. Figure 13-2 compares the variable speed performance map from Fig. 10-38 with a predicted performance map for a seven-row linear stagger angle distribution (inlet guide vane and six stators). It can be seen that variable geometry offers a significant improvement in surge margin compared to variable speed operation at flow rates less than the design flow.

Figure 13-3 illustrates the influence of the number of adjustable blade rows when the linear adjustment distribution is used for this compressor. Increasing N has the expected effect of greater flow capacity control. It can be noted that the best surge margin appears to be associated with $N = 7$. Generally, there is an optimum value of N to enhance the surge margin, typically around one-half of the total number of stationary rows available for adjustment, excluding exit guide vanes, which are ineffective for this purpose. In this case, there are eleven rows available (inlet guide vane and ten stators), so an optimum N around 6 might be

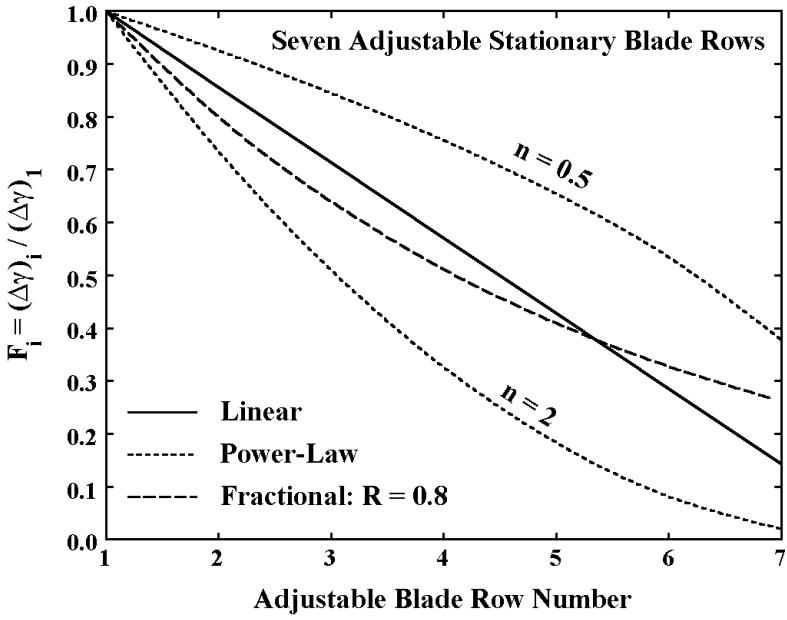

FIGURE 13-1 Alternate Adjustment Strategies

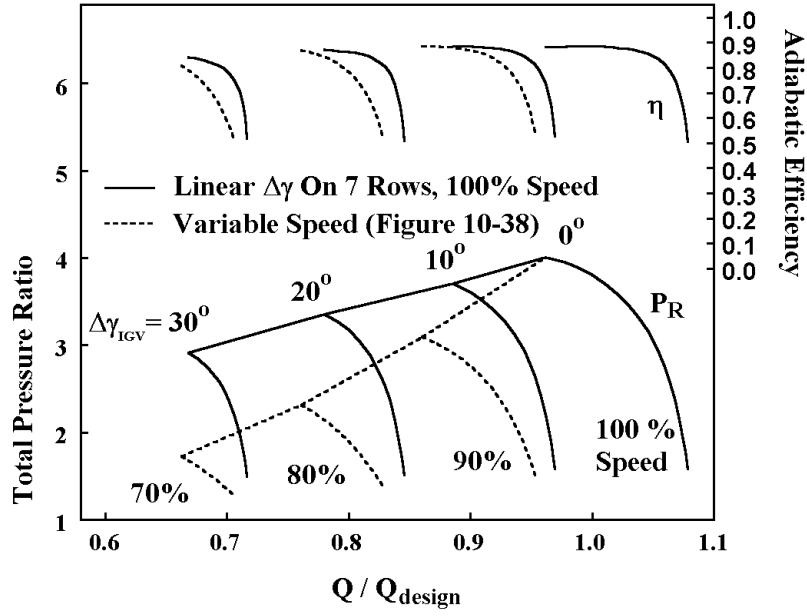

FIGURE 13-2 Variable Geometry and Variable Speed

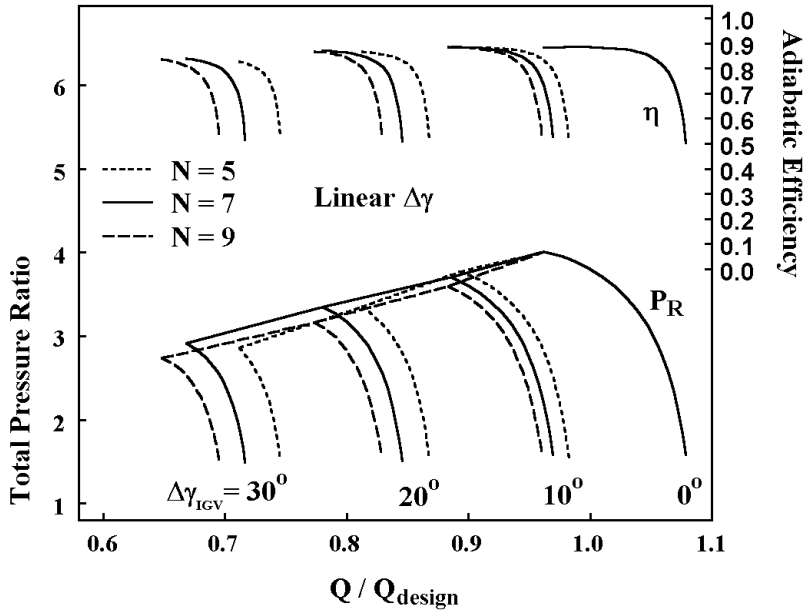

FIGURE 13-3 Influence of *N* with Linear $\Delta\gamma$

expected. This really follows from the mechanism by which variable geometry improves surge margin. Basically, the adjustable blades close down the front stages, which would normally stall at the lower flows, to shift the load to the rear stages. Stated differently, adjustable blades reduce the load on the front stages to permit operation at lower volume flow rates where the rear stages will operate closer to their design conditions. Hence variable geometry in the rear stages is seldom effective for this purpose.

Figure 13-4 illustrates the fractional adjustment distribution for a series of values of R. It can be seen that increasing R results in increased capacity control, while yielding essentially identical surge lines for all values considered. But there is a slight adverse effect on surge margin and on efficiency with increasing R, suggesting that larger values would not be good for this compressor. As a general rule, $R \approx 0.8$ is usually a good choice for the fractional adjustment distribution.

Figure 13-5 illustrates the influence of N with the fractional distribution with $R = 0.8$. Increasing N from 5 to 7 increases both capacity control and surge margin. But only two values of N are shown, since the surge estimate for the higher value is based on stall in one of the adjustable blade rows. Hence, adding more adjustable blade rows with the fractional adjustment distribution on this compressor cannot further improve the surge margin. Comparing Figs. 13-3 and 13-5 shows that the fractional adjustment distribution can achieve a surge margin improvement comparable to the linear style for this compressor.

It can be concluded that the use of adjustable stationary blade rows is a very powerful method for achieving increased surge margin at volume flow rates less

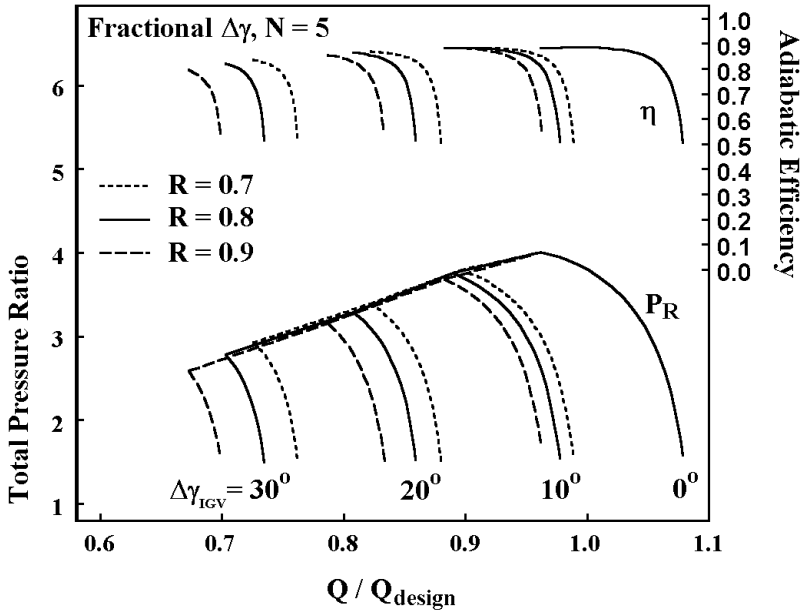

FIGURE 13-4 Influence of *R* with Fractional $\Delta\gamma$

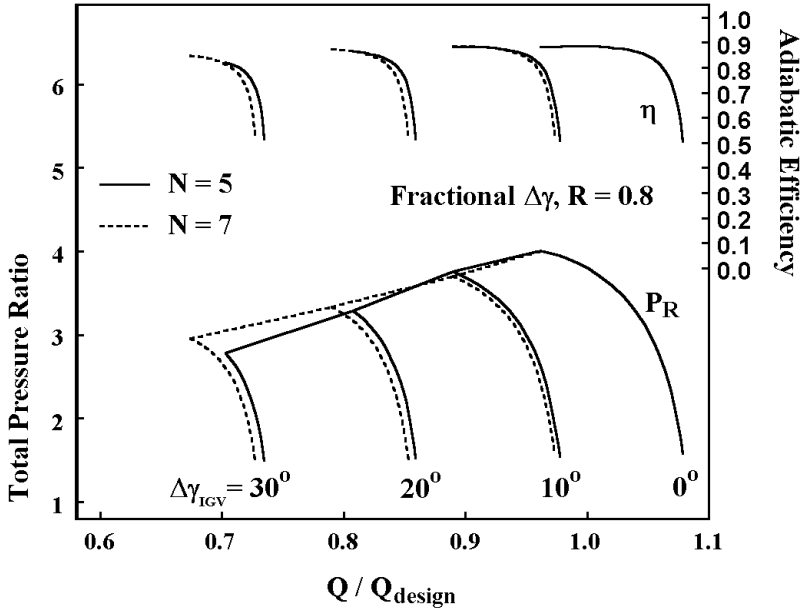

FIGURE 13-5 Influence of *N* with Fractional $\Delta\gamma$

than the design value. By including the provision to impose these adjustments within the aerodynamic performance analysis, it is relatively simple to arrive at an appropriate adjustment distribution style and the appropriate number of adjustable blade rows to be used. This also makes it rather easy to generate a predicted performance map to evaluate a range of adjustable blade row settings. The alternative of accomplishing these adjustments manually on each blade row can make this a very tedious process, with little likelihood of arriving at an optimum choice.

13.2 THE EXHAUST DIFFUSER

The industrial axial-flow compressor normally supplies the compressed gas to some process through an exit pipe flange. Often, the final destination will involve redirecting the flow from the axial flow leaving the compressor to a pipe oriented normal to the compressor axis. Hence the overall performance of the compressor is strongly influenced by the performance of the exhaust-end components. Generally, the flow is first diffused in an exhaust diffuser to recover some of the kinetic energy in the form of static pressure. This may be an annular, axial exhaust diffuser such as that shown in figure 13-6. Alternatively, curved diffusers may be used to redirect the flow in the radial direction for collection by a scroll or collector, such as illustrated in figure 13-7. Consequently, a very wide variety of exhaust diffusers may be employed, requiring a very general performance analysis technique.

One aerodynamic performance analysis method that can handle these various configurations is the vaneless passage analysis of Aungier (1993, 2000). That analysis has been extensively qualified for centrifugal compressor performance

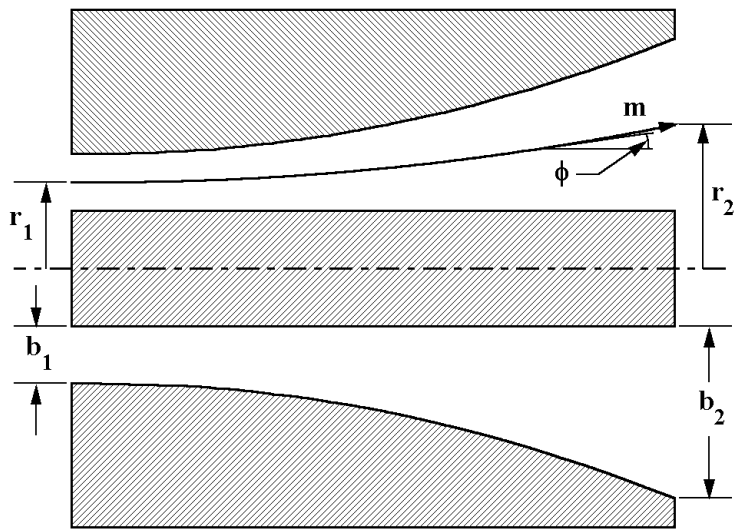

FIGURE 13-6 Axial Exhaust Diffuser Geometry

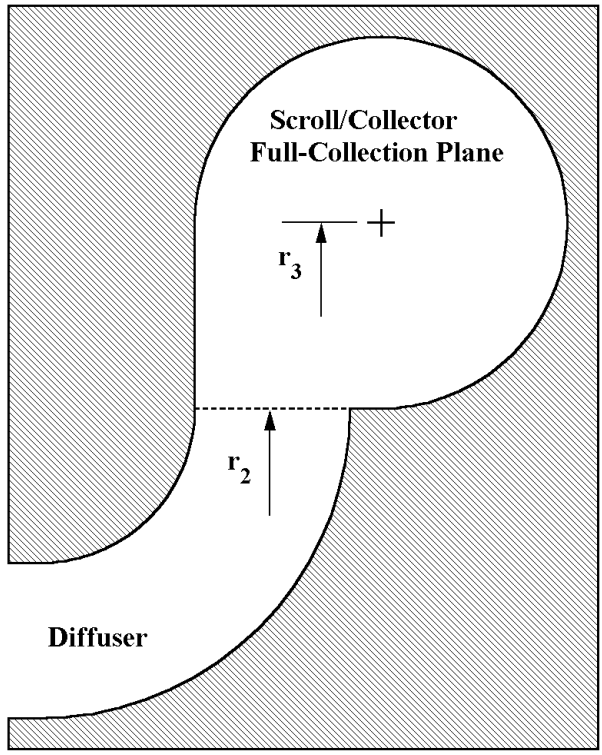

FIGURE 13-7 Curved Exhaust Diffuser

analysis, where it has been used to treat the swirling flows in vaneless diffusers and 180° crossover bends. With one minor modification, it is directly applicable to the axial-flow compressor exhaust diffuser problem. The area requiring modification is the modeling of the end-wall boundary layer growth and the associated viscous blockage effects. For axisymmetric flow in centrifugal compressors, the rather ideal form of the tangential velocity profile in the boundary layer makes that profile an obvious choice to estimate boundary layer growth. But that choice is not appropriate for an axial-flow compressor exhaust diffuser, which is likely to have little or no tangential velocity component. Similarly, viscous blockage effects are less critical in the centrifugal compressor. Cases where substantial blockage may be induced by excessive rates of diffusion generally occur only in the crossover bend, where performance is primarily described by total thermodynamic conditions rather than static. If the total pressure loss is predicted with sufficient accuracy, the overall performance predictions are relatively insensitive to the viscous blockage prediction. Again, the axial-flow compressor exhaust diffuser often involves quite different requirements. A simple dump collector may be used to collect the flow following an axial exhaust diffuser, such that little or

none of the kinetic energy is recovered. Thus, static conditions can be extremely important, requiring a more careful consideration of viscous blockage effects. Fortunately, generalization of the centrifugal compressor vaneless passage performance analysis proved to be relatively straightforward, since most of the fundamental models were already included for the purpose of total pressure loss prediction. The modified analysis used for axial-flow compressor exhaust diffusers is presented in this section.

The analysis is a mean-streamline or one-dimensional flow analysis with wall friction and empirical corrections for diffusion and curvature effects. Figure 13-6 illustrates the mean streamline in a typical axial exhaust diffuser configuration and the nomenclature used in the analysis. The governing equations for one-dimensional flow with skin friction are developed in Aungier (1993, 2000) as

$$2\pi rb\rho C_m(1-B) = \dot{m} \tag{13-5}$$

$$bC_m \frac{d(rC_\theta)}{dm} = -rCC_\theta c_f \tag{13-6}$$

$$\frac{1}{\rho}\frac{dP}{dm} = \frac{C_\theta^2 \sin\phi}{r} - C_m \frac{dC_m}{dm} - \frac{CC_m c_f}{b} - \frac{dI_D}{dm} - I_C \tag{13-7}$$

$$H = h + \tfrac{1}{2}C^2 \tag{13-8}$$

The blockage, B, specifies the fraction of the passage area unavailable for the inviscid through flow, due to viscous effects. The skin friction coefficient, c_f, supplies a correction for the effect of the wall shear stress, τ_w.

$$c_f = \frac{\tau_w}{\frac{1}{2}\rho C^2} \tag{13-9}$$

The terms I_D and I_C are introduced in Aungier (1993, 2000) to account for losses due to diffusion and passage curvature, respectively. In other respects, this set of equations follows directly from the governing equations for inviscid flow presented in Chapter 3, when simplified to time-steady, axisymmetric, one-dimensional flow in a stationary coordinate system.

From classical two-dimensional diffuser technology (e.g., Reneau et al., 1966) it is known that the low loss regime is closely related to the well-known diffuser divergence angle, $2\theta_C$. This parameter can be generalized to annular diffusers by

$$2\theta_C = 2\tan^{-1}[b_1(A_2/A_1 - 1)/(2L)] \tag{13-10}$$

The nomenclature shown in Fig. 13-6, where L is the length of the mean streamline and $A = 2\pi rb$ is the passage area, is used. Aungier (1993, 2000) introduces a divergence parameter, D, defined as

$$D = 2\tan\theta_C = b_1(A_2/A_1 - 1)/L \tag{13-11}$$

The experimental results in Fig. 8(b) of Reneau et al. (1967) show that diffusion losses are low when $D < D_m$, where

$$D_m = 0.4(b_1 / L)^{0.35} \tag{13-12}$$

Aungier (1993, 2000) uses an analogy with the classical diffuser parameters, D and D_m, but defined as local diffusion parameters, i.e.,

$$D = -\frac{b}{C}\frac{dC}{dm} \tag{13-13}$$

$$D_m = 0.4\cos\beta(b_1 / L)^{0.35} \tag{13-14}$$

Based on detailed comparisons with predicted and measured losses in a substantial number of centrifugal compressor vaneless diffusers, an empirical model was developed for a diffusion efficiency parameter, E, in the form

$$E = 1\,;\, D \le 0 \tag{13-15}$$

$$E = 1 - 0.2(D / D_m)^2\,;\, 0 < D < D_m \tag{13-16}$$

$$E = 0.8\sqrt{D_m / D}\,;\, D \ge D_m \tag{13-17}$$

Then the streamwise diffusion term in Eq. (13-7) is given by

$$\frac{dI_D}{dm} = -2(P_t - P)(1 - E)\frac{1}{\rho C}\frac{dC}{dm} \tag{13-18}$$

It was necessary to check for excessive diffusion in the meridional direction as well as the streamwise direction, again using an analogy with classical diffuser technology. The maximum stall-free local passage area, A_m, is estimated from

$$A_m = A_1[1 + 0.1925m / b_1] \tag{13-19}$$

which corresponds to a local divergence angle limit of $2\theta_C \approx 11°$. The highly swirling flows in centrifugal compressors required a slightly more conservative limit of 9°, but that is considered unnecessary for the exhaust diffuser application. A minimum value of I_D is estimated when $A > A_m$

$$I_D \ge 0.65(P_t - P)[1 - A_m / A] / \rho \tag{13-20}$$

This value is imposed as a lower limit on I_D obtained by integrating Eq. (13-18). The passage curvature, κ_m, is used to estimate I_C as

$$I_C = |\kappa_m|(P_t - P)C_m / (13\rho C) \tag{13-21}$$

$$\kappa_m = -\frac{d\phi}{dm} \tag{13-22}$$

Aungier (1993, 2000) employs simple one-seventh power law velocity profiles as the boundary layer approximation. This continues to be used, since a one-dimensional flow analysis really does not provide an adequate basis for modeling boundary layer shape factors in any reasonable fashion. As noted, it is not possible to rely on the wall friction effects on the tangential momentum balance as a basis for estimating boundary layer growth in an exhaust diffuser. Instead, the meridional velocity profile is used with a simple flat-plat boundary layer growth model, including adjustment for variations in radius and the boundary layer edge meridional momentum. Turbulent boundary layer growth along a flat plate can be estimated from (Pai, 1957)

$$\frac{d\delta}{dm} \approx 5c_f \tag{13-23}$$

This is generalized to the annular passage with two end-wall boundary layers in the form

$$\frac{d[rb\rho C_m^2(2\delta / b)]}{dm} = 10c_f \rho rCC_m \tag{13-24}$$

The radius and the boundary layer edge meridional momentum corrections in this equation are similar to momentum thickness corrections of Eq. (3-43). This follows from the approximation that the boundary layer shape factor is constant, which requires that the ratio of the boundary layer thickness to the momentum thickness be constant. The boundary layer thicknesses estimated from Eq. (13-24) must be limited by the fully developed viscous flow profile condition, i.e., $2\delta \le b$.

The fractional area blockage due to the two end-wall boundary layers will be designated as B_{BL}. The boundary layer blockage for one-seventh power law profiles can be shown to be

$$B_{BL} = (2\delta / b) / 8 \tag{13-25}$$

For the exhaust diffuser, it must also be recognized that viscous blockage may increase substantially if the rate of diffusion becomes excessive, i.e., if the maximum stall-free local passage area, A_m, is exceeded. If that occurs, it is assumed that further diffusion of C_m is suppressed by a minimum blockage, B_{SEP}, where

$$B_{SEP} = 0 \; ; A \le A_m \tag{13-26}$$

$$B_{SEP} = 1 - A_m / A \; ; A > A_m \tag{13-27}$$

B_{SEP} can be imposed as a lower limit on the blockage estimated from Eq. (13-25), but it has been found that a smooth transition between these two values is obtained from the following empirical equation:

$$B = 1 - (1 - B_{SEP})(1 - B_{BL} + B_{SEP}^2) \tag{13-28}$$

Equations (13-24) through (13-28) contain all of the modifications to the original analysis of Aungier (1993, 2000) developed specifically for the exhaust diffuser application.

Finally, solution of the governing equations requires a model for the skin friction coefficient. Following Aungier (2000), a generalized pipe friction factor model is employed for this purpose. While that models fully developed pipe or channel flow, it is applicable to boundary layers by replacing the pipe diameter (or channel width) with 2δ. For this problem, the relevant Reynolds number is

$$\mathrm{Re} = \frac{2\rho C \delta}{\mu} \tag{13-29}$$

The other parameter required is the peak-to-valley surface roughness height, e. Usually surface roughness is measured as a root-mean-square value, e_{rms}. The two values can be approximately related by assuming a sine-wave variation for the roughness to yield

$$e = e_{rms} / 0.3535 \tag{13-30}$$

If Re is less than 2000, the laminar skin friction coefficient applies.

$$c_f = c_{fl} = 16 / \mathrm{Re} \tag{13-31}$$

When $Re > 2000$ and the wall is smooth ($e = 0$), the well-known log-law profile yields

$$\frac{1}{\sqrt{4c_{fs}}} = -2\log_{10}\left[\frac{2.51}{\mathrm{Re}\sqrt{4c_{fs}}}\right] \tag{13-32}$$

In the limit when the flow is turbulent and the wall is fully rough,

$$\frac{1}{\sqrt{4c_{fr}}} = -2\log_{10}\left[\frac{e}{3.71(2\delta)}\right] \tag{13-33}$$

The experimental results of Nikuradse (1930), show that surface roughness becomes significant when

$$\mathrm{Re}_e = (\mathrm{Re} - 2000)e / (2\delta) > 60 \tag{13-34}$$

Hence, a general turbulent skin friction coefficient is given by

$$c_{ft} = c_{fs}; \mathrm{Re}_e < 60 \tag{13-35}$$

$$c_{ft} = c_{fs} + (c_{fr} - c_{fs})(1 - 60 / \mathrm{Re}_e);\ \mathrm{Re}_e \geq 60 \tag{13-36}$$

If $Re \geq 4000$, c_f is defined by Eq. (13-35) or (13-36). For $2000 < Re < 4000$, the flow is in the transition zone and the skin friction coefficient is approximated by

$$c_f = c_{fl} + (c_{ft} - c_{fl})(\mathrm{Re} / 2000 - 1) \tag{13-37}$$

These empirical equations yield values in very close agreement with the experimental results of Nikuradse (1930).

The performance analysis of the exhaust diffuser involves integrating Eqs. (13-5) through (13-8) along the diffuser length, supported by the supplemental relations provided in this section. Input specifications required include the passage geometry, mass flow rate and inlet values of the total thermodynamic conditions, tangential velocity and normalized boundary layer thickness, $2\delta / b$. To show at least a qualitative evaluation of the method, the experimental data for two-dimensional diffusers of Reneau et al (1967) will be used. In general, two-dimensional and annular diffusers perform in a reasonably similar manner as long as appropriate dimensionless parameters are used in any comparison. In particular, the diffuser divergence angle definition of Eq. (13-10) should be used. The highest inlet blockage level results in Fig. 4(d) of Reneau et al. (1967) are the most representative of exhaust diffusers. These show an optimum static pressure recovery coefficient, c_p, around $L / b_1 \approx 0.8$ and $A_2 / A_1 \approx 2.4$, as well as a strong variation of c_p with both diffuser divergence angle and area ratio. The static pressure recovery coefficient is defined as

$$c_p = (P_2 - P_1) / (P_{t1} - P_1) \tag{13-38}$$

The exhaust diffusers for the analysis were specified with a constant radius hub wall and a conical shroud wall. The inlet boundary layer thickness was defined as $2\delta / b = 0.4$ to match the experimental inlet blockage of $B_1 = 0.05$. The inlet tangential velocity was set to zero, and the other inlet data were selected to produce the Mach number and Reynolds number levels indicate in the reference. Figures 13-8 and 13-9 show comparisons of results that pass close to the optimum performance condition and illustrate the influence of variations in both $2\theta_C$ and A_2/A_1. Clearly the performance analysis shows reasonable agreement with the experimental results. Although this is a rather qualitative evaluation, it seems evident that the analysis adapted from centrifugal compressor technology should be applicable to the evaluation of exhaust diffusers for axial-flow compressors. From its use in centrifugal compressors, it is also known to be applicable to more general diffuser configurations, such as the curved diffuser illustrated in Fig. 13-7.

13.3 THE SCROLL OR COLLECTOR

For industrial axial-flow compressors, the flow from the diffuser may be collected in a scroll or a collector and discharged into an exit pipe. Figure 13-7 presents the side-view schematic of a curved diffuser discharging into a scroll or a collector.

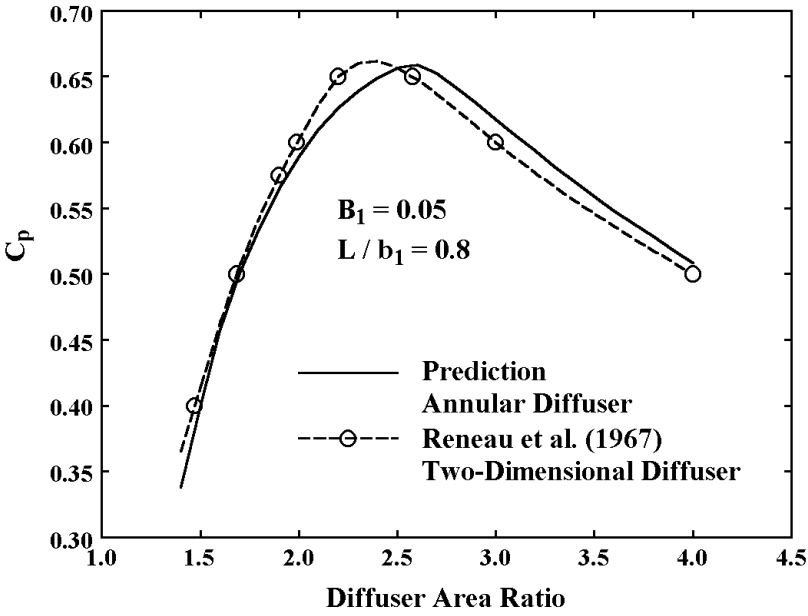

FIGURE 13-8 Influence of Area Ratio on c_p

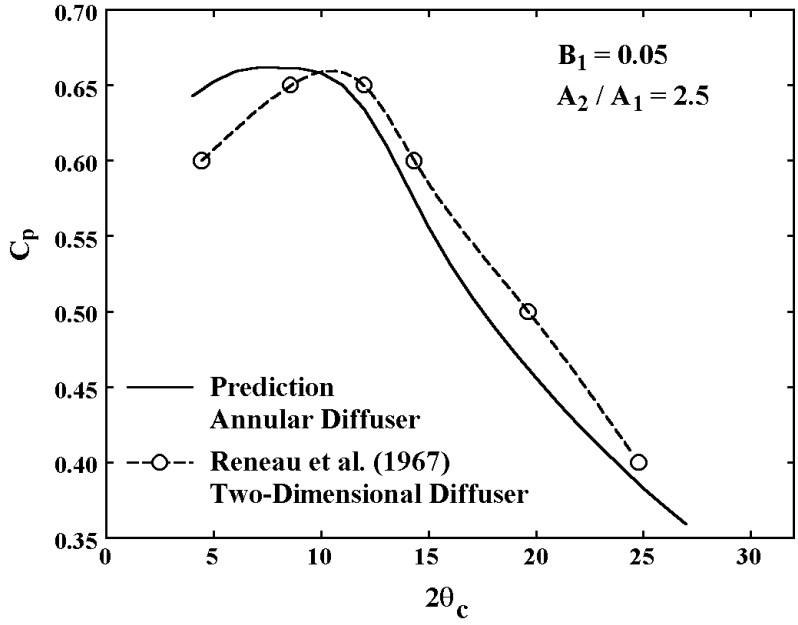

FIGURE 13-9 Influence of Divergence Angle on c_p

Figure 13-10 shows the front view of a scroll, where the area increases in the circumferential direction. By contrast, a collector has a circumferentially uniform passage area. Figure 13-11 is a schematic of an axial exhaust diffuser with a collector similar to the arrangement used on the NASA 10-stage compressor (Budinger and Thomson, 1952).

The performance of scrolls and collectors can be evaluated using models developed for centrifugal compressors (Aungier, 2000). All flow conditions are known at the entrance station, 2, from the exhaust diffuser exit conditions. The next key location is designated as station 3, which is the cross-section where the flow has been completely collected, as shown in Fig. 13-10. The flow is then discharged through an exit cone to the exit flange, station 4. The velocity at stations 3 and 4 are computed from conservation of mass. For simplicity, the gas density will be assumed to be constant in the scroll or collector. While that is not a necessary assumption, Mach number levels are almost always sufficiently low to justify its use in estimating the loss coefficient. Hence

$$C_3 = C_{m2} A_2 / A_3 \tag{13-39}$$

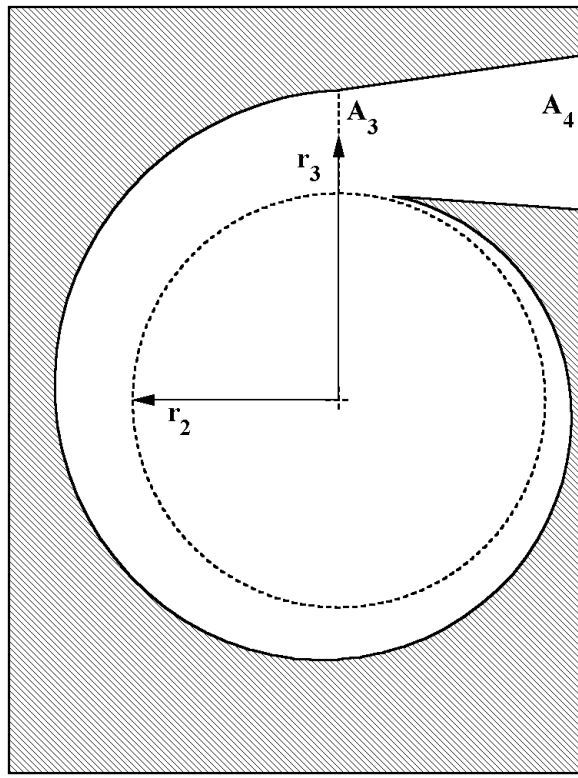

FIGURE 13-10 Side View of a Scroll

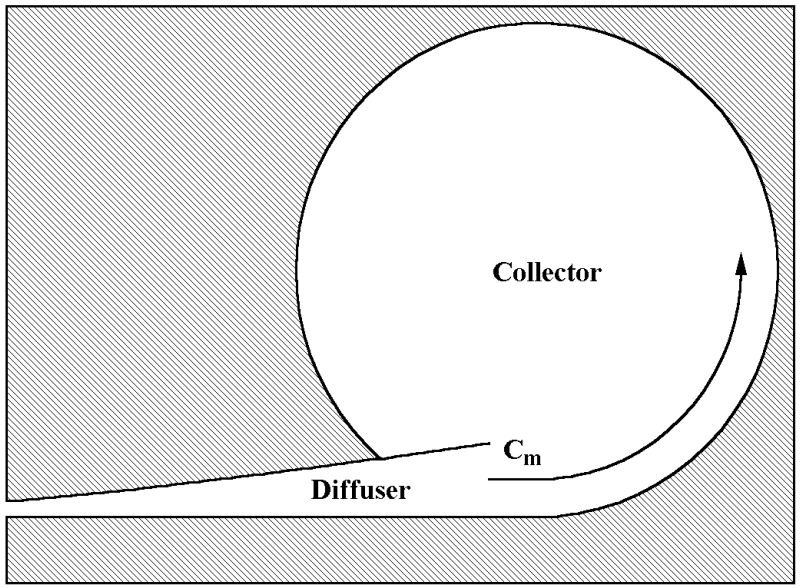

FIGURE 13-11 An Axial Diffuser and Collector

$$C_4 = C_{m2} A_2 / A_4 \tag{13-40}$$

The overall total pressure loss coefficient for the scroll or collector is defined as

$$\overline{\omega} = (P_{t2} - P_{t4}) / (P_{t2} - P_2) \tag{13-41}$$

This loss coefficient is computed as the sum of four component loss coefficients. First, it is assumed that the meridional velocity head entering the scroll or collector will be lost. The meridional component of the velocity will develop into a secondary flow pattern in the scroll or collector, as illustrated in Fig. 13-11, and eventually dissipate as a loss. Hence the meridional loss coefficient is given by

$$\overline{\omega}_m = (C_{m2} / C_2)^2 \tag{13-42}$$

The tangential component of velocity can be smoothly recovered in a properly sized scroll. The ideal size is determined by requiring conservation of angular momentum between stations 2 and 3, i.e.,

$$r_3 C_3 = r_2 C_{\theta 2} \tag{13-43}$$

A sizing parameter, *SP*, is defined as

$$SP = r_2 C_{\theta 2} / (r_3 C_3) \tag{13-44}$$

SP = 1 is the ideal sizing condition. *SP* > 1 indicates an oversized scroll that is attempting to overdiffuse the flow relative to the ideal condition. *SP* < 1 is an undersized scroll that is attempting to accelerate the flow relative to the ideal condition. The tangential loss coefficient is given by

$$\overline{\omega}_\theta = \frac{1}{2}\frac{r_3 C_3^2}{r_2 C_2^2}[SP^2 - 1];\ SP \geq 1 \tag{13-45}$$

$$\overline{\omega}_\theta = \frac{r_3 C_3^2}{r_2 C_2^2}[SP - 1]^2;\ SP < 1 \tag{13-46}$$

Equations (13-45) and (13-46) are the same as those used in Aungier (2000), but Eq. (13-44) has been used to remove a singularity at *SP* = 0 in the original reference. Unlike in the centrifugal compressor, $C_{\theta 2}$ = *SP* = 0 is a condition likely to be encountered in an axial-flow compressor. In the case of a collector, the equations for the tangential loss coefficient apply only to the full collection station. When a constant passage area collector first starts to collect the flow, the passage area is greatly oversized, such that the collector attempts to diffuse the tangential velocity essentially to zero, which implies the local SP becomes infinite. A corresponding tangential loss coefficient can be computed by combining Eqs. (13-44) and 13-45) and taking the limit as *SP* approaches infinity. The collector tangential loss coefficient is set to an average of the two extreme values, i.e.,

$$(\overline{\omega}_\theta)_{coll} = \frac{\overline{\omega}_\theta}{2} + \frac{r_2 C_{\theta 2}^2}{2 r_3 C_2^2} \tag{13-47}$$

A wall skin friction loss coefficient is given by

$$\overline{\omega}_{sf} = 4 c_f (C_3 / C_2)^2 L / d_H \tag{13-48}$$

L is the average path length of the flow in the scroll and d_H is the mean hydraulic diameter of the passage.

$$L = \pi(r_2 + r_3)/2 \tag{13-49}$$

$$d_H = \sqrt{2A_3/\pi} \tag{13-50}$$

The conventional definition of hydraulic diameter is four times the passage area divided by the wetted perimeter of the passage. That is used in Eq. (13-50),

assuming that the cross-section of the passage is circular and the mean passage area is one-half of A_3. For a constant passage area collector, the relations used are

$$L = \pi r_3 \tag{13-51}$$

$$d_H = \sqrt{4A_3 / \pi} \tag{13-52}$$

The skin friction coefficient is calculated in the same fashion as that for the exhaust diffuser, but with the Reynolds number and surface roughness referenced to d_H rather than 2δ. Finally, an exit cone loss coefficient is given by

$$\overline{\omega}_{ex} = [(C_3 - C_4) / C_2]^2 \; ; C_3 > C_4 \tag{13-53}$$

$$\overline{\omega}_{ex} = 0 \; ; C_3 \leq C_4 \tag{13-54}$$

The overall total pressure loss coefficient and exit total pressure for the scroll or collector are given by

$$\overline{\omega}_{sc} = \overline{\omega}_m + \overline{\omega}_\theta + \overline{\omega}_{sf} + \overline{\omega}_{ex} \tag{13-55}$$

$$P_{t4} = P_{t2} - \overline{\omega}_{sc}(P_{t2} - P_2) \tag{13-56}$$

Conservation of energy and an appropriate equation of state from Chapter 2 yields $H_4 = H_2 = H(T_{t2}, P_{t2})$, from which $T_{t4} = T(P_{t4}, H_2)$. Then a simple mass balance on A_4 yields the discharge velocity and static conditions. The scroll or collector static pressure recovery coefficient is given by

$$c_{psc} = (P_4 - P_2) / (P_{t2} - P_2) \tag{13-57}$$

An overall exhaust system loss coefficient and static pressure recovery coefficient for the diffuser and the scroll or collector combined can also be calculated, i.e.,

$$\overline{\omega} = (P_{t1} - P_{t4}) / (P_{t1} - P_1) \tag{13-58}$$

$$c_p = (P_4 - P_1) / (P_{t1} - P_1) \tag{13-59}$$

One useful application of the performance analysis results is to define a discharge loss coefficient for use by the axial-flow compressor performance analysis of Chapter 9. That analysis basically predicts the compressor's performance up to the diffuser entrance, i.e., the station 1 data in the notation in this chapter. A discharge pressure can be computed as

$$P_{dis} = P_{t1} - \overline{\omega}_{dis}(P_{t1} - P_1) \tag{13-60}$$

The appropriate definition of the discharge loss coefficient depends on whether a total-to-total or a total-to-static evaluation is appropriate, i.e., whether or not the kinetic energy at the discharge is valuable to the application served by the compressor. In the case of total-to-total evaluation, Eq. (13-58) provides the appropriate definition. In the case of total-to-static evaluation, the appropriate discharge loss coefficient definition is

$$\bar{\omega}_{dis} = 1 - c_p \tag{13-61}$$

where c_p is given by Eq. (13-59).

13.4 REYNOLDS NUMBER AND SURFACE ROUGHNESS EFFECTS

The exhaust diffuser performance analysis provides a good basis to discuss methods to include the effects of surface roughness on axial-flow compressor performance. This is often an important consideration for industrial centrifugal compressors, which accounts for its detailed treatment in the exhaust system analyses adapted from centrifugal compressor technology. Surface finish effects are much less likely to be important in typical axial-flow compressor applications. Hence, Reynolds number correction models from the literature seldom considered it [e.g., the models in Chapter 6 and in Wassell (1968)]. But it can become significant for applications involving very high Reynolds numbers or very poor surface finishes. Fortunately, there is a fairly simple method to externally impose a correction for surface roughness on any Reynolds number correction model. This can be easily accomplished by limiting the Reynolds number used in the correction to values for which the surfaces involved are hydraulically smooth. A reasonable approximation for this purpose is to limit the Reynolds number used in the correction by

$$\mathrm{Re}_d \le 60 d / e \tag{13-62}$$

where d is the characteristic length dimension used to define the Reynolds number. Figure 13-12 applies this simple method to correct the skin friction coefficient from Eq. (13-32) and compares it to results from Eqs. (13-30) through (13-37). Clearly, this simple correction is in rather good agreement with the more precise empirical model derived from the pipe friction factor charts of Nikuradse (1930).

13.5 THE AXIAL-CENTRIFUGAL COMPRESSOR

The axial-centrifugal compressor consists of a series of axial-flow compressor stages followed by a centrifugal compressor stage. Under appropriate circumstances, this can offer definite advantages. Centrifugal compressor design and analysis is covered in depth in Aungier (2000). The discussion here is limited to

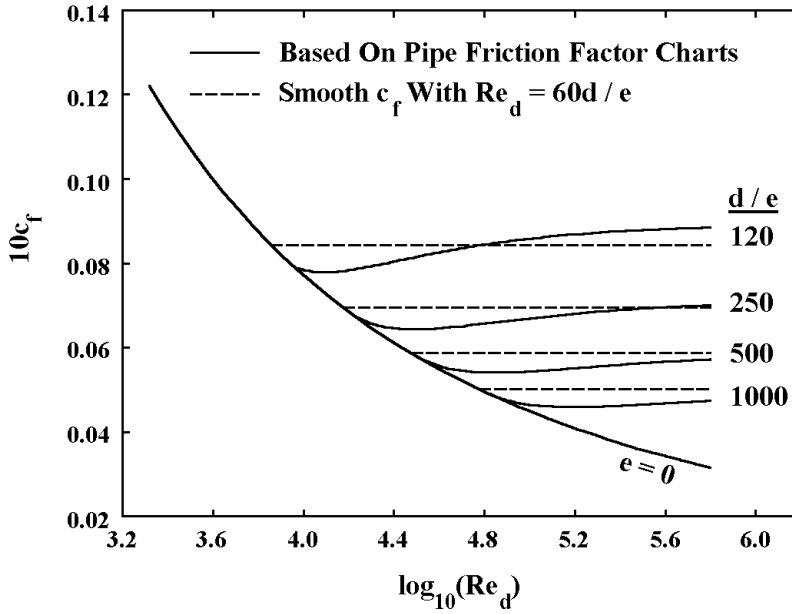

FIGURE 13-12 Simple Surface Roughness Correction

the concept of combining the two compressor types. The relative merits and characteristics of the axial-flow compressor and the centrifugal compressor were discussed briefly in Chapter 1. To review, the following are key differences between these two types of compressors:

- The axial-flow compressor can achieve significantly higher mass flow rates per unit frontal area.
- The centrifugal compressor can achieve significantly larger pressure ratios per stage.
- The centrifugal compressor is generally the more rugged and lower-cost compressor type.
- The axial-flow compressor generally offers higher efficiency, although the centrifugal compressor has become rather competitive in recent years.
- The centrifugal compressor offers stable operation over a much wider mass flow range.
- The axial-flow compressor offers a much steeper pressure-mass flow characteristic.
- The centrifugal compressor is much better suited to matching with a scroll or collector at the discharge.

These differences need definite qualification when considering a combination of the two types in a single compressor. Axial-flow and centrifugal compressor

stages achieve their optimum performance at quite different dimensionless performance parameters. This difference is typically expressed in terms of specific speed or the characteristic stage inlet flow coefficient, ϕ_0. The latter should not be confused with the definition of flow coefficient, ϕ, used earlier in this book. Here, the characteristic stage inlet flow coefficient is defined as

$$\phi_0 = \dot{m} / (\pi r_{tip}^2 U_{tip} \rho_{t0}) \tag{13-63}$$

Figure 13-13 shows stage efficiency levels that should be achievable with optimized centrifugal compressor stages as a function of ϕ_0. It is adapted from generalized performance charts in Aungier (2000) to emphasize simple radial discharge centrifugal stages. Operation at higher values of ϕ_0 is certainly possible, but is likely to require a mixed-flow design to achieve adequate efficiency levels. A mixed-flow design is a compromise between axial-flow and radial-flow styles such that the flow exits the impeller with velocity components in both the axial and radial directions. At sufficiently high values of ϕ_0, an axial-flow stage will be required. A meaningful extension of the chart in Fig. 13-13 to cover mixed flow and axial-flow stages is not available. Balje (1981) presents a specific speed chart intended to include the three compressor stage types. But his use of total-to-static efficiency severely limits the value of his chart as a guide for multi-stage compressor design. In Chapter 10, it was noted that many investigators now favor relatively low stage flow coefficients, ϕ, around 0.5. The flow

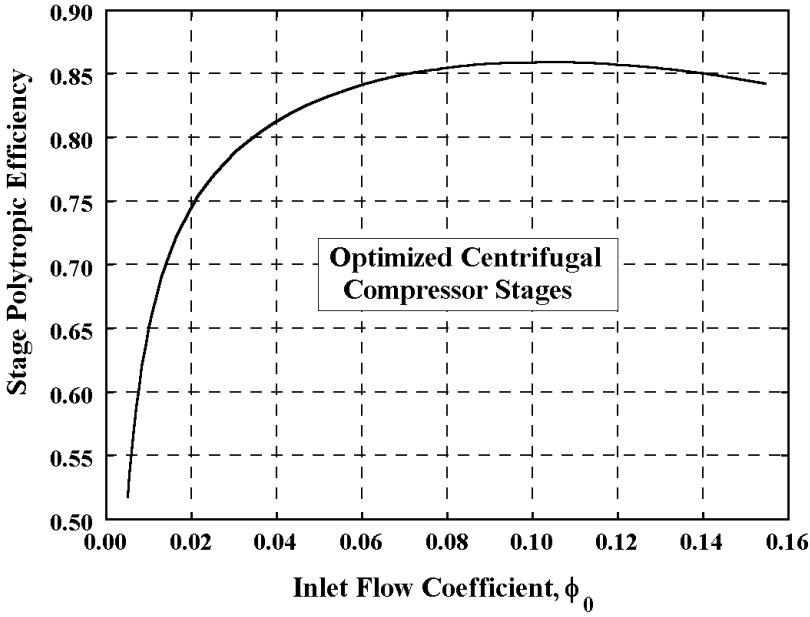

FIGURE 13-13 Centrifugal Stage Performance

coefficients ϕ_0 and ϕ can be approximately related using the stage hub-to-shroud radius ratio, ε.

$$\phi_0 \approx \tfrac{1}{2}(1-\varepsilon^2)(1+\varepsilon)\phi \tag{13-64}$$

$$\varepsilon = r_h / r_s \tag{13-65}$$

Typical values of ε for front stages in a compressor are in the 0.4 to 0.6 range. From Eq. (13-64) this suggests that ϕ_0 in the range of about 0.25 to 0.3 are about the lowest values to be expected for optimized axial-flow stages. The stage efficiency is expected to be essentially unaffected by variation of ε from 0.4 to 0.6, yet it results in substantial variation in ϕ_0. Indeed, ϕ_0 is rather ambiguous as a guide to achievable efficiency levels for axial-flow stages. In the rear stages of an axial-flow compressor, ε may become large enough to produce values of ϕ_0 in the range normal for centrifugal stages. But in that case, the performance of an axial-flow stage is likely to be far from optimum due to aspect ratio effects associated with the very short blades.

It is clear that axial-flow stages generally operate at values of ϕ_0 that are considerably higher than centrifugal stages. In addition, a centrifugal stage substituted for an axial-flow stage will normally operate at a lower value of ϕ_0 than the axial-flow stage it replaced. This follows from the fact that r_{tip} and U_{tip} will typically be greater for the centrifugal stage. Consequently, it may be beneficial to replace some of the rear axial-flow stages in an axial-flow compressor with a centrifugal stage. The higher stage pressure ratio offered by the centrifugal stage may permit replacement of several axial-flow stages to substantially reduce cost. If aspect ratio effects are significant in the replaced axial-flow stages, performance may also be improved. It is rather easy to evaluate the potential benefits from this approach. Simply compute ϕ_0 in the rear stages and estimate r_{tip} of a replacement centrifugal stage to compute ϕ_0 for the centrifugal stage. If the upstream axial-flow stages have reduced ϕ_0 to a value suitable for a centrifugal stage, the replacement may be appropriate. The expected centrifugal stage efficiency can be estimated from Fig. 13-13, or by using the more refined charts or the performance analysis in Aungier (2000).

Some industrial axial-flow compressor designers believe that a final centrifugal stage is beneficial, even without obtaining a cost or performance benefit directly from the substitution. This may involve using a rather modest pressure-ratio centrifugal stage primarily to reduce the exhaust system losses. It is clear that a scroll or collector following typical axial-flow stages cannot be well-matched, since the sizing parameter of Eq. (13-44) will always be close to zero. Hence the scroll or collector will always be grossly undersized. There is little that can be done in terms of scroll or collector design except to minimize the harm done to the performance by the tangential loss and exit cone loss. Hence the designer's ability to minimize the exhaust system loss is primarily limited to the exhaust diffuser design. It can be argued that a centrifugal stage can efficiently turn the flow to the radial direction to permit the design of a radial diffuser with a well-matched scroll or collector. No doubt there is some merit to that approach, although it may be difficult to quantify. If the axial length available is limited, e.g., to favor rotor dynamics, the benefit may be more obvious. For example, if

space limitations require reducing the length of the axial diffuser of Fig. 13-11 or replacing it with the curved diffuser of Fig. 13-7, the alternative of a final centrifugal stage may be easier to justify.

EXERCISES

13.1 Flow exits an exhaust diffuser with $C_\theta = 0$. What will be the minimum possible value of the loss coefficient for a scroll or collector following the diffuser? What options do you have to minimize this loss coefficient? Of the diffuser types shown in Figs. 13-7 and 13-11, which one yields the lowest loss in the scroll/collector?

13.2 A curved diffuser similar to that of Fig. 13-7 is replaced by a very low pressure-ratio centrifugal stage with a vaneless diffuser. The diffuser has an exit passage area and radius identical to the original diffuser and the scroll sizing parameter is 1. This substitution reduces the scroll total pressure loss coefficient from 1.1 to 0.4. What can you conclude about the overall exhaust system losses for the two configurations? Which contributions to the overall loss are likely to be reduced by this substitution? What steps are needed to justify this substitution?

13.3 Assuming the diffusers of Figs. 13-7 and 13-11 have the same inlet and discharge areas and $C_\theta = 0$, which diffuser is likely to have the lower loss? Under what circumstances would you choose the higher loss configuration? Would your answers be different if $C_\theta > 0$?

13.4 A general Reynolds number correction model is applied to correct low Reynolds number test performance to high Reynolds number operating conditions. Surface roughness is found to be significant, so the approximate correction of Section 13.4 is imposed. How confident can you be in the results? What areas of uncertainty need to be considered?

13.5 Polishing blade and end-wall surfaces to improve surface finish can add significant cost to the manufacturing process. How can you use the skin friction coefficient model of Eqs. (13-30) through (13-37) to determine whether the added cost is justified? How would you adapt this procedure when the characteristic length is not a passage width or diameter (e.g., blade chord Reynolds number)?